

Early Galaxy Formation and the Hubble Tension

Stacy McGaugh¹ 

¹ Department of Astronomy, Case Western Reserve University; stacy.mcgough@case.edu

Abstract: A tension between the expansion rate of the universe obtained from direct measurements and that inferred from fits to the acoustic power spectrum of the Cosmic Microwave Background (CMB) radiation has emerged as higher multipoles have been incorporated into CMB fits. This temporal evolution is suggestive of a systematic effect at fine angular scales, and may be related to the observation of unexpectedly massive galaxies at high redshift. Such objects could cause anomalous gravitational lensing of the surface of last scattering, which in turn may affect the best-fit value of H_0 . If so, the Hubble tension may be the result of a systematic effect in the fitting of CMB data rather than a systematic error in local measurements.

Keywords: Early universe; Galaxy formation; Large-scale structure of the universe

1. Concordance Cosmology

The concordance cosmology (Λ CDM) emerged in the 1990s thanks to observational advances that constrained a broad variety of cosmological parameters [1,2]. These led to the surprising recognition that the mass density was less than the critical density [3], in conflict with then-standard SCDM cosmology and Inflationary theory. Retaining the latter implied a second surprise in the form of the cosmological constant such that $\Omega_m + \Omega_\Lambda = 1$, which in turn predicted that the expansion rate of the universe would currently be *accelerating* [4]. This unlikely-seeming prediction was subsequently observed in the Hubble diagram of Type Ia SN [5,6]. This picture was further corroborated by the location of the first peak of the acoustic power spectrum of the CMB being consistent with a flat ($\Omega_k = 0$) Robertson-Walker geometry [7,8].

The range of concordance parameters narrowed with the completion of the Hubble Space Telescope Key Project to Measure the Hubble Constant [9], and a ‘vanilla’ set of Λ CDM parameters emerged with¹ $h = 0.7$ and $\Omega_m = 0.3$ [10] some twenty years ago. Since that time, a tension [11–13] has emerged between direct measurements of the Hubble constant [9,14–20] and that obtained from fits to the acoustic power spectrum of the cosmic microwave background obtained by the Planck mission [21]. This tension was not present in earlier data from WMAP [22]. Indeed, one of the most persuasive arguments in favor of vanilla Λ CDM was the concordance of WMAP cosmological parameters with other observations, especially H_0 . Now that a tension has emerged, it is natural to ask when and where things went amiss.

To this end, it is interesting to update the Ω_m - H_0 concordance diagram that was pivotal in establishing Λ CDM in the first place [2]. Figure 1 shows modern values of the same constraints used in Ref. [2] nearly three decades ago. These include the SH0ES direct measurement of the Hubble constant $H_0 = 73.04 \pm 1.04 \text{ km s}^{-1} \text{ Mpc}^{-1}$ [19], the shape parameter $\Gamma = \Omega_m h = 0.168 \pm 0.016$ from large scale structure [23], the baryon fraction of clusters of galaxies $\Omega_m h^{1/2} = 0.221 \pm 0.031$ [24], and the age of the globular cluster M92, $13.80 \pm 0.75 \text{ Gyr}$ [25]. For the age constraint, we assume a flat geometry as an open universe without a cosmological constant would be too young to have a concordance region. For simplicity, we also assume the age of the universe is indistinguishable from the age of the globular cluster, which presumably formed very early, and surely within the first 750 Myr (the uncertainty in its age).

¹ $h = H_0 / (100 \text{ km s}^{-1} \text{ Mpc}^{-1})$.



Citation: McGaugh, S. Hubble Tension. *Preprints* 2022, 1, 0. <https://doi.org/>

Publisher’s Note: MDPI stays neutral with regard to jurisdictional claims in published maps and institutional affiliations.



Copyright: © 2022 by the author. Licensee MDPI, Basel, Switzerland. This article is an open access article distributed under the terms and conditions of the Creative Commons Attribution (CC BY) license (<https://creativecommons.org/licenses/by/4.0/>).

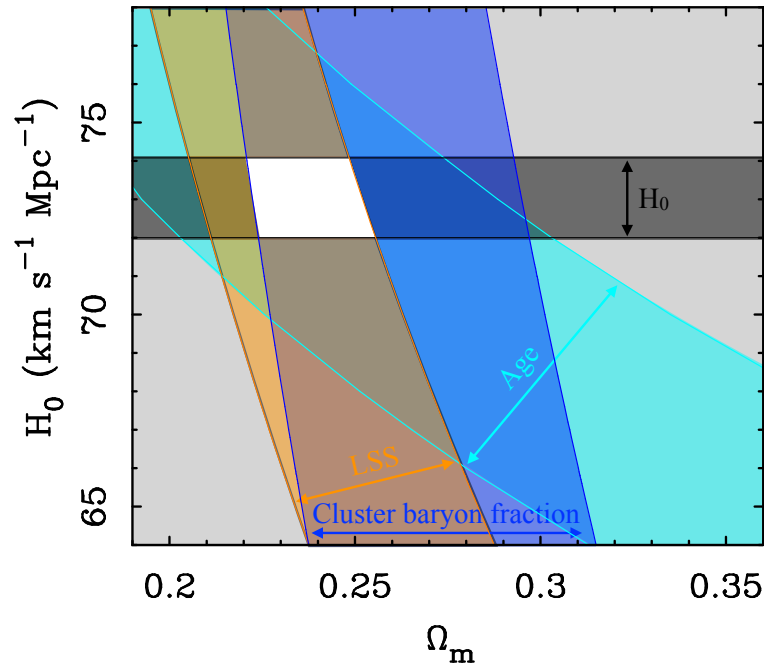


Figure 1. The concordance region (white space) in Ω_m - H_0 space [2] where the allowed regions (colored bands) of many constraints intersect. Illustrated constraints include a direct measurement of the Hubble constant [19, black], the age of a flat universe containing the globular cluster M92 [25, light blue], the cluster baryon fraction [24, dark blue], and the shape parameter from large scale structure [23, orange].

The data in Fig. 1 tell very much the same story as it has for the entirety of this century. Taking these observations at face value, we recover a concordance cosmology with $\Omega_m = 0.235 \pm 0.015$ and $h = 0.7304 \pm 0.0104$. This is completely consistent with the WMAP3 [22] cosmology ($\Omega_m = 0.241 \pm 0.034$, $h = 0.732 \pm 0.032$), but less so with later results.

The most accurate constraint in Fig. 1 is the direct measurement of the Hubble constant [19], so it is worth considering what happens if we adopt other values. If we take $H_0 = 69.8 \pm 0.8 \text{ km s}^{-1} \text{ Mpc}^{-1}$ [14], then together with the other constraints, we obtain $\Omega_m = 0.247 \pm 0.017$. This remains consistent with early WMAP cosmologies despite the lower value of the Hubble constant. If we take a higher value, $H_0 = 74.6 \pm 0.8$ [20], then $\Omega_m = 0.233 \pm 0.013$, consistent with local estimates of the mass density [26,27]. The plausible range of mass density based on modern measurements of the same observational constraints that established the concordance cosmology in the first place is $0.22 \leq \Omega_m \leq 0.264$. This is consistent with all WMAP cosmologies but not with the $\Omega_m = 0.315 \pm 0.007$ of the Planck cosmology [21]. Tension is thus not restricted to the Hubble constant, it also appears in the mass density. A tension also appears in the power spectrum normalization σ_8 [28–30] and the baryon density [31] in the form of a tension between deuterium and lithium [32]. Indeed, it is possible to find indications of tensions in any cosmological parameter; the trick is to avoid confirmation bias in assessing the credibility of each.

2. Covariance and the Hubble Tension

Fig. 2 summarizes the status of the Hubble tension as of this writing. The best fit to the Planck CMB data, $H_0 = 67.36 \pm 0.54 \text{ km s}^{-1} \text{ Mpc}^{-1}$ [21], clearly differs from the bulk of the accurate “local” determinations [9,14–20], which range from 69 to 75 $\text{km s}^{-1} \text{ Mpc}^{-1}$ obtained by a variety of methods and calibrations. This subject is the focus of much research with frequent updates to essentially the same result, e.g., Freedman *et al.* [14] and Freedman [33], so we restrict Fig. 2 to a single entry from each distinct group. Accuracy matters, so we also highlight measurements with statistical uncertainties $\leq 3 \text{ km s}^{-1} \text{ Mpc}^{-1}$. The

weighted mean of these values gives $H_0 = 73.24 \pm 0.38 \text{ km s}^{-1} \text{ Mpc}^{-1}$. This differs from the Planck value by nearly 9σ , so formally the tension is real.

The above assessment is both straightforward and naive, as it ignores systematic errors, which are difficult to quantify. An assessment of systematics is built into the SH0ES error bar [19], so by their assessment, the tension remains highly significant (5σ). Ref. [17] excludes $H_0 < 70.5 \text{ km s}^{-1} \text{ Mpc}^{-1}$ at 95% c.l.; if anything, their probability distribution skews to higher rather than lower H_0 . A local systematic calibration uncertainty of $\pm 1.3 \text{ km s}^{-1} \text{ Mpc}^{-1}$ is suggested by Ref. [34]; adopting this still implies a $\sim 4\sigma$ tension. As always, the question is how much to believe these assessments [12,13].

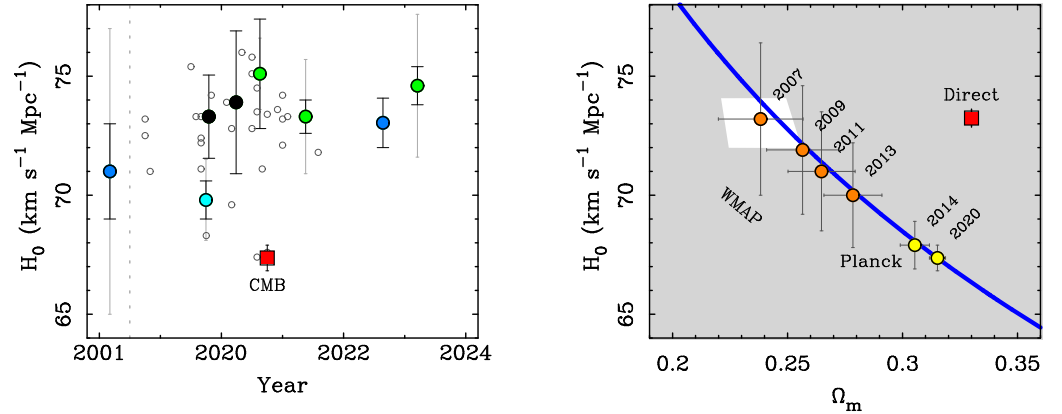


Figure 2. Recent direct measurements of H_0 [11] over time (left) including the earlier HST key project [9, far left]. Measurements with statistical uncertainties $\leq 3 \text{ km s}^{-1} \text{ Mpc}^{-1}$ from independent groups are color coded by calibrator: geometry [black: 15,16], Cepheids [blue: 9,19], TRGB [cyan: 14], or a combination [green: 17,18,20]. Statistical and systematic uncertainties are shown as dark and light error bars, respectively; these are omitted for less accurate data (small open circles). Determinations of H_0 from WMAP [22,35–37, orange] and Planck [21,38, yellow] covary with the mass density as $\Omega_m h^3 = 0.09633 \pm 0.00030$ [bold line, 21], and have decreased steadily over time. For comparison, the red square shows the latest CMB value in the left panel and the mean of the accurate direct determinations in the right panel (at arbitrary Ω_m). The concordance region from Fig. 1 is shown as the open region in the right panel; the grey region is excluded by those data.

The history of the distance scale predisposes us to suspect a systematic error somewhere in the calibration of the distance ladder. This view is encouraged by the apparent tension between Cepheid [19] and TRGB [14] calibrations. However, there is no tension between these two calibrators in other analyses [17,18,20]. There are also geometric methods [15,16] that are independent of these calibrators. The essential answer has not changed since the completion of the completion of the Hubble Space Telescope Key Project to Measure the Hubble Constant [9], but the accuracy has improved to the point that it is difficult to sustain the presumption that there must be a systematic error in the distance scale [12].

Local measurements of the distance scale and fits to the CMB measure completely different things. The local measurements are all some realization of the traditional Hubble program in which distances and redshifts to nearby galaxies are measured, and the slope of the velocity–distance relation is obtained. This is an empirical procedure. In contrast, fits to the power spectrum of the CMB at $z = 1090$ are model (Λ CDM) dependent, and the results are sensitive to all of the cosmic parameters simultaneously with inevitable covariance. The strongest covariances affecting the Hubble parameter is with the mass density. These covary in CMB fits approximately as $\Omega_m h^3 = 0.09633 \pm 0.00030$ [21].

The covariance of H_0 with Ω_m is apparent in Fig. 2. There is also a correlation with time: the best-fit combination has marched steadily along the trench of constant $\Omega_m h^3$ from $H_0 = 73.2 \pm 3.2 \text{ km s}^{-1} \text{ Mpc}^{-1}$ [22] to $H_0 = 67.36 \pm 0.54 \text{ km s}^{-1} \text{ Mpc}^{-1}$ [21]. It is the CMB

result that has progressively deviated from the concordance Λ CDM region established around the turn of the millennium, not local measurements.

The temporal progression of the best-fit values of H_0 and Ω_m is a flag that suggests something systematic in the CMB analyses rather than traditional Hubble constant determinations. The latter scatter approximately as expected: the rms variation of the accurate data in Fig. 2 is $1.78 \text{ km s}^{-1} \text{ Mpc}^{-1}$ while the size of the statistical uncertainties anticipate that it should be $1.55 \text{ km s}^{-1} \text{ Mpc}^{-1}$. This implies that systematic uncertainties are not contributing much to the scatter, though one must always be cautious of a calibration issue that would translate all results without affecting the scatter [34].

The CMB data from independent experiments are in good agreement where they overlap, so the temporal progression is not a measurement error. What has changed over time is the availability of data on ever finer scales, tracing the power spectrum to higher multipoles ℓ . Something subtle seems to be tipping the covariance of parameters to favor lower H_0 along the trench of constant $\Omega_m h^3$ as higher ℓ have been incorporated into the fits.

3. Bright Galaxies at High Redshift

An important recent development is the observation of unexpectedly massive galaxies at high redshift. This may seem unrelated at first, but CMB data have reached the level of precision where the subtle effects of gravitational lensing by masses intervening between ourselves and the surface of last scattering cannot be ignored. If massive galaxies assembled anomalously early, then gravitational lensing by these objects may have a systematic impact on CMB fits.

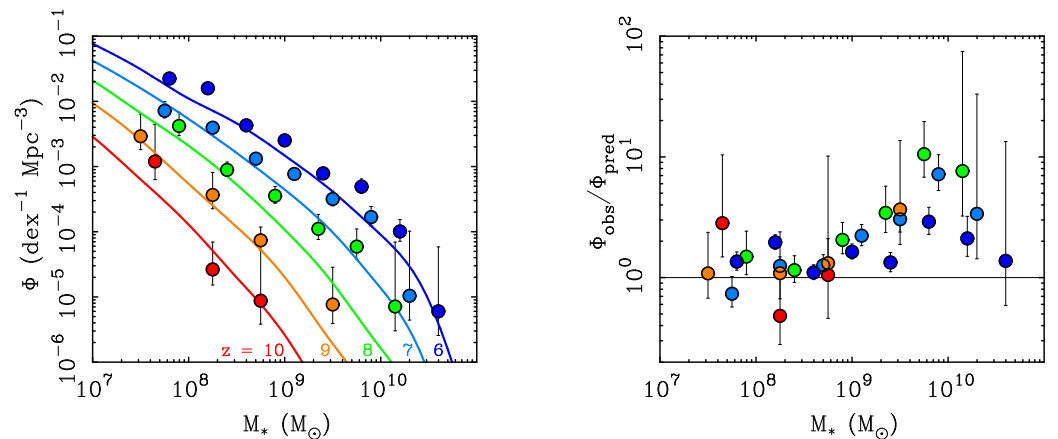


Figure 3. The number density of galaxies as a function of their stellar mass, color coded by redshift, as labeled. The left panel shows predicted stellar mass functions [39, lines] with the corresponding data [40, circles]. The right panel shows the ratio of the observed to predicted density of galaxies. There is a clear excess of massive galaxies at high redshifts.

Galaxies are expected to assemble gradually through the hierarchical merger of many progenitors in Λ CDM. This process takes a long time. A typical massive galaxy is predicted to have assembled half its stars around $z \approx 0.7$ when the universe is ~ 7 Gyr old, roughly half its current age [41,42]. In contrast, there are many galaxies that are observed to be massive and already quiescent at $z \approx 3$ [43–46] when the universe is only ~ 2 Gyr old. These appear to have formed half of their stars in the first gigayear ($z \gtrsim 6$), and are consistent with the traditional picture of a monolithic early type galaxy that formed early ($z \geq 10$) and followed an approximately exponential star formation history with a short (~ 1 Gyr) e-folding time [44]. This comes as a surprise² to the predictions of hierarchical structure formation in Λ CDM [48,49].

² The formation of massive galaxies at $z \geq 10$ was predicted in advance by Bob Sanders [47].

Though highlighted by recent JWST observations [50–55], the discrepancy is already apparent by $z \approx 3$ [43,44]. Figure 3 illustrates the situation shortly before the launch of JWST. The observed luminosity function of galaxies broadly resembles the predicted evolution, but there is a systematic excess of bright, massive galaxies. This persists over all redshifts $z > 3$ and holds in all environments, both in clusters and in the field [44].

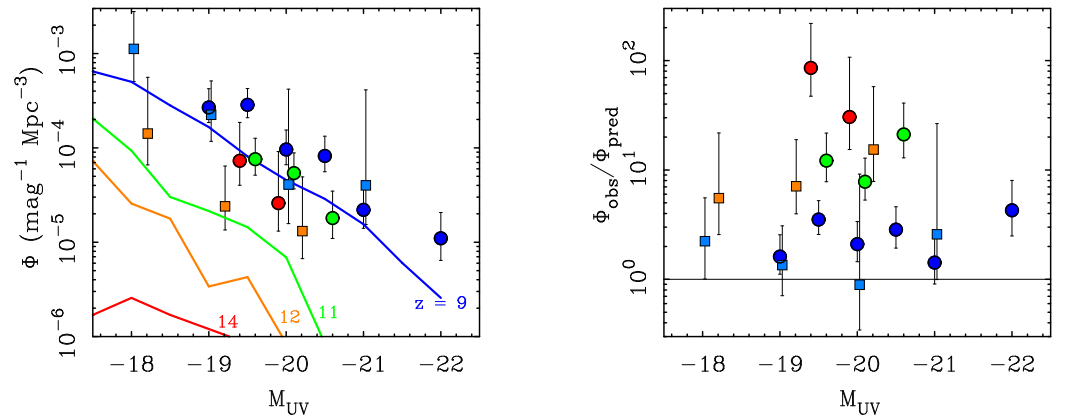


Figure 4. The number density of galaxies as a function of their ultraviolet absolute magnitude observed by JWST at very high redshift. The left panel shows predicted luminosity functions [56, lines], color coded by redshift, as labeled. Data in the corresponding redshift bins are shown as squares [57] or circles [58]. The right panel shows the ratio of the observed to predicted density of galaxies. The observed luminosity function barely evolves, in contrast to the prediction of substantial evolution as the first dark matter halos assemble. There is a large excess of bright galaxies at the highest redshifts observed.

The impossibly early galaxy problem [43] has become more severe with new observations from JWST, extending to $z > 9$ (Fig. 4). Over this redshift range, the luminosity function is predicted to evolve rapidly [56]. There is a good physical reason for this: this is the epoch of hierarchical mass assembly in Λ CDM, when fragmentary protogalaxies should first be forming before subsequently assembling into more massive galaxies — hence the ragged luminosity functions in the highest redshift³ bins. There is not sufficient time to assemble the observed mass into single objects [48,49].

These JWST results are new, and will no doubt be debated for some time. Valid concerns can be raised over the veracity of photometric redshifts and the relation of ultraviolet starlight to dark matter halo mass. However, the anomalous presence of early massive galaxies found by JWST corroborates previous work for which spectroscopic redshifts are available and for which the assessment of stellar mass is robust. It is therefore hard to avoid the conclusion that galaxies grew too big too fast.

4. Gravitational Lensing of the CMB

The presence of massive galaxies in the early universe is an anomaly to the Λ CDM structure formation paradigm. They should not be there [48,49]. The existence of such galaxies violates the assumptions that underpin fits to the acoustic power spectrum of the CMB, so may lead to systematic errors in the assessment of cosmological parameters based on those fits. In particular, the calculation of gravitational lensing would be impacted [59].

Gravitational lensing of the surface of last scattering by intervening masses is an effect that becomes important at high ℓ , beginning to impact the fit for $\ell > 800$. Intriguingly, restricting the fit of the Planck data to $\ell < 800$ returns a higher Hubble constant [21] consistent with that found by WMAP [37], which only probed scales where lensing matters

³ A luminosity density of $\sim 7 \times 10^{-6} \text{ mag}^{-1} \text{ Mpc}^{-3}$ is estimated at $z \approx 16$ [57]. This point is omitted from Fig. 4 because the corresponding prediction is not a number: galaxies bright enough to observe should not yet exist.

little. So perhaps there is a systematic effect due to the gravitational lensing of the surface of last scattering.

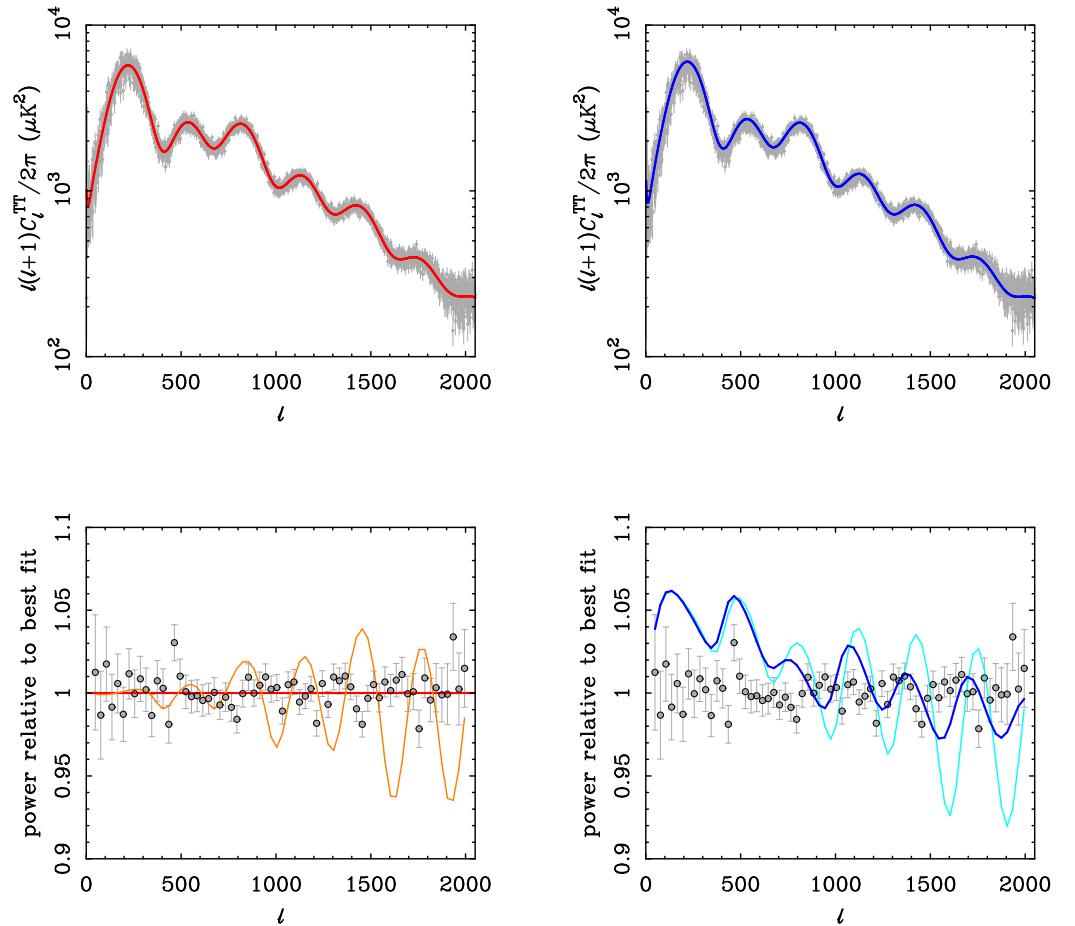


Figure 5. Top: unbinned Planck data [60] with the best-fit power spectrum (left) and a model with $H_0 = 73 \text{ km s}^{-1} \text{ Mpc}^{-1}$ (right) with Ω_{CDM} scaled to keep $\Omega_m h^3 = 0.09633$ constant. Bottom: the ratio of binned data and model to the best fit. The darker line is the model including the expected effects of lensing; the lighter line is the power spectrum emergent from the surface of last scattering before lensing. If there is an anomalous source of lensing from massive early galaxies then the mapping from emergent to observed power spectrum will be miscalculated and the best-fit cosmological parameters will be in error.

We have seen above that massive galaxies appear anomalously early in the history of the universe. This implies a stronger lensing effect than expected. In order to compute the effects of lensing on the observed CMB, lensing potentials are extrapolated forward in time by assuming linear growth of the perturbations observed in the CMB. This assumption is hardwired into the calculations used to fit CMB data. This implies that the computation of lensing underestimates the real effect by assuming a growth rate that is less than observed.

High mass galaxies at high redshift are anomalous, so we do not know how to calculate the lensing potentials they represent. We can, however, use CAMB [61] to compute the CMB power spectrum to see how the predicted power varies in the absence of this effect. We do this in Fig. 5, which compares the Planck best fit with a model that has $H_0 = 73 \text{ km s}^{-1} \text{ Mpc}^{-1}$. We scale the mass density of this model to maintain consistency with the constraint $\Omega_m h^3 = 0.09633$ [21]. We hold the mass density of baryons and neutrinos constant, scaling that of cold dark matter to $\Omega_{\text{CDM}} h^2 = 0.109$ for a total mass density of $\Omega_m = 0.248$, consistent with the concordance region in Fig. 1. This gives an acoustic power

spectrum that is only distinguishable from the best-fit version upon close scrutiny (Fig. 5), at a level where the effect of gravitational lensing is perceptible.

We can see in Fig. 5 that the Planck fit [21] is indeed the better fit. We can also see that the lensing calculation, though subtle, plays an important role in the fit. Lensing blurs the surface of last scattering, suppressing some of the oscillations that were emergent at the time of recombination, as illustrated by the lighter lines in the lower panels of Fig. 5. If the predicted amount of lensing is wrong because of the anomalously early appearance of massive galaxies, the resulting fit will be systematically in error.

The power spectrum of the model with $H_0 = 73 \text{ km s}^{-1} \text{ Mpc}^{-1}$ is offset and tilted from the Planck best fit. The offset at $\ell < 800$ is mostly caused by covariance with the optical depth to the surface of last scattering, which shifts the amplitude. WMAP found $\tau = 0.089 \pm 0.014$ [37], rather higher than the best fit of Planck, $\tau = 0.0544 \pm 0.0073$ [21]. This is about what it takes to shift the model into agreement with the data at low ℓ , which is part of why WMAP found that to be the best fit at the time. There are, of course, other covariances as well, especially with the amplitude of the power spectrum, σ_8 , which itself is in some tension with local measurements [28–30].

In addition to blurring the surface of last scattering, gravitational lensing also adds a source of small scale power to the observed fluctuations that are not present in the power spectrum emergent from the surface of last scattering. This will add poorly correlated power at high ℓ . If there is an excess of such power from anomalously early galaxies, it will tilt the power spectrum in the sense seen in Fig. 5. That is, if one starts with a model like that with $H_0 = 73 \text{ km s}^{-1} \text{ Mpc}^{-1}$, power will be added at high ℓ beyond what can be explained by the model. If this happens but we are unaware of it, the fitting procedure will indulge the covariance of all the cosmological parameters until a fit is found. Driving H_0 down and Ω_m up goes in the right direction to do this. It is therefore conceivable that the Planck best-fit H_0 is in systematic error due to anomalous gravitational lensing.

5. Conclusions

Cosmological parameters obtained from fits to the acoustic power spectrum of the cosmic microwave background have gradually moved away from the concordance region specified by independent constraints, moving steadily along the trench of constant $\Omega_m h^3$ to lower H_0 and higher Ω_m . This migration has resulted in the current tension with the locally measured value of the Hubble constant. We point out that this migration correlates with the inclusion of higher multipoles in the fits, for which the effects of gravitational lensing are important. The appearance of anomalously massive galaxies in the early universe as indicated by JWST (and other) observations suggests that the impact of gravitational lensing on the CMB may be underestimated. It is conceivable that this is a contributing factor to the temporal migration of the best-fit cosmological parameters and the resulting Hubble tension. If so, it may be the CMB value of H_0 that is systematically in error rather than local determinations.

Massive galaxies at high redshift is anomalous in Λ CDM and would require new physics to explain. We have refrained from speculating on what such new physics might be [47,62]. In addition to specifying a particular hypothesis for the new physics, it would further be necessary to incorporate it into a Boltzmann code in order to calculate the lensing effect on the surface of last scattering. Such a calculation is beyond the scope of this work.

Funding: This research has been supported in part by NSF grant PHY-1911909 and NASA grant 80NSSC19K0570.

Data Availability Statement: Data and models are available at the author's websites: astroweb.case.edu/ssm/data and astroweb.case.edu/ssm/models.

Conflicts of Interest: The author declares no conflict of interest.

Abbreviations

The following abbreviations are used in this manuscript:

CMB	Cosmic Microwave Background
JWST	James Webb Space Telescope
Λ CDM	Lambda Cold Dark Matter
SCDM	Standard Cold Dark Matter
WMAP	Wilkinson Microwave Anisotropy Probe

References

- Efstathiou, G.; Sutherland, W.J.; Maddox, S.J. The cosmological constant and cold dark matter. *Nature* **1990**, *348*, 705–707. <https://doi.org/10.1038/348705a0>.
- Ostriker, J.P.; Steinhardt, P.J. The observational case for a low-density Universe with a non-zero cosmological constant. *Nature* **1995**, *377*, 600–602. <https://doi.org/10.1038/377600a0>.
- Davis, M.; Efstathiou, G.; Frenk, C.S.; White, S.D.M. The end of cold dark matter? *Nature* **1992**, *356*, 489–494. <https://doi.org/10.1038/356489a0>.
- McGaugh, S.S. Cosmological constant. *Nature* **1996**, *381*, 483. <https://doi.org/10.1038/381483b0>.
- Riess, A.G.; Filippenko, A.V.; Challis, P.; Clocchiatti, A.; Diercks, A.; Garnavich, P.M.; Gilliland, R.L.; Hogan, C.J.; Jha, S.; Kirshner, R.P.; et al. Observational Evidence from Supernovae for an Accelerating Universe and a Cosmological Constant. *AJ* **1998**, *116*, 1009–1038, [arXiv:astro-ph/astro-ph/9805201]. <https://doi.org/10.1086/300499>.
- Perlmutter, S.; Aldering, G.; Goldhaber, G.; Knop, R.A.; Nugent, P.; Castro, P.G.; Deustua, S.; Fabbro, S.; Goobar, A.; Groom, D.E.; et al. Measurements of Ω and Λ from 42 High-Redshift Supernovae. *ApJ* **1999**, *517*, 565–586, [arXiv:astro-ph/astro-ph/9812133]. <https://doi.org/10.1086/307221>.
- de Bernardis, P.; Ade, P.A.R.; Bock, J.J.; Bond, J.R.; Borrill, J.; Boscaleri, A.; Coble, K.; Crill, B.P.; De Gasperis, G.; Farese, P.C.; et al. A flat Universe from high-resolution maps of the cosmic microwave background radiation. *Nature* **2000**, *404*, 955–959, [arXiv:astro-ph/astro-ph/0004404]. <https://doi.org/10.1038/35010035>.
- Page, L.; Nolta, M.R.; Barnes, C.; Bennett, C.L.; Halpern, M.; Hinshaw, G.; Jarosik, N.; Kogut, A.; Limon, M.; Meyer, S.S.; et al. First-Year Wilkinson Microwave Anisotropy Probe (WMAP) Observations: Interpretation of the TT and TE Angular Power Spectrum Peaks. *ApJS* **2003**, *148*, 233–241, [arXiv:astro-ph/astro-ph/0302220]. <https://doi.org/10.1086/377224>.
- Freedman, W.L.; Madore, B.F.; Gibson, B.K.; Ferrarese, L.; Kelson, D.D.; Sakai, S.; Mould, J.R.; Kennicutt, Jr., R.C.; Ford, H.C.; Graham, J.A.; et al. Final Results from the Hubble Space Telescope Key Project to Measure the Hubble Constant. *ApJ* **2001**, *553*, 47–72, [arXiv:astro-ph/0012376]. <https://doi.org/10.1086/320638>.
- Tegmark, M.; Strauss, M.A.; Blanton, M.R.; Abazajian, K.; Dodelson, S.; Sandvik, H.; Wang, X.; Weinberg, D.H.; Zehavi, I.; Bahcall, N.A.; et al. Cosmological parameters from SDSS and WMAP. *Phys. Rev. D* **2004**, *69*, 103501, [arXiv:astro-ph/astro-ph/0310723]. <https://doi.org/10.1103/PhysRevD.69.103501>.
- Di Valentino, E.; Mena, O.; Pan, S.; Visinelli, L.; Yang, W.; Melchiorri, A.; Mota, D.F.; Riess, A.G.; Silk, J. In the realm of the Hubble tension—a review of solutions. *Classical and Quantum Gravity* **2021**, *38*, 153001, [arXiv:astro-ph.CO/2103.01183]. <https://doi.org/10.1088/1361-6382/ac086d>.
- Tully, R.B. The Hubble Constant: A Historical Review. *arXiv e-prints* **2023**, p. arXiv:2305.11950, [arXiv:astro-ph.CO/2305.11950]. <https://doi.org/10.48550/arXiv.2305.11950>.
- Cervantes-Cota, J.L.; Galindo-Uribarri, S.; Smoot, G.F. The Unsettled Number: Hubble’s Tension. *Universe* **2023**, *9*, 501, [arXiv:physics.hist-ph/2311.07552]. <https://doi.org/10.3390/universe9120501>.
- Freedman, W.L.; Madore, B.F.; Hatt, D.; Hoyt, T.J.; Jang, I.S.; Beaton, R.L.; Burns, C.R.; Lee, M.G.; Monson, A.J.; Neeley, J.R.; et al. The Carnegie-Chicago Hubble Program. VIII. An Independent Determination of the Hubble Constant Based on the Tip of the Red Giant Branch. *ApJ* **2019**, *882*, 34, [arXiv:astro-ph.CO/1907.05922]. <https://doi.org/10.3847/1538-4357/ab2f73>.
- Wong, K.C.; Suyu, S.H.; Chen, G.C.F.; Rusu, C.E.; Millon, M.; Sluse, D.; Bonvin, V.; Fassnacht, C.D.; Taubenberger, S.; Auger, M.W.; et al. HOLICOW - XIII. A 2.4 per cent measurement of H_0 from lensed quasars: 5.3 σ tension between early- and late-Universe probes. *MNRAS* **2020**, *498*, 1420–1439, [arXiv:astro-ph.CO/1907.04869]. <https://doi.org/10.1093/mnras/stz3094>.
- Pesce, D.W.; Braatz, J.A.; Reid, M.J.; Riess, A.G.; Scolnic, D.; Condon, J.J.; Gao, F.; Henkel, C.; Impellizzeri, C.M.V.; Kuo, C.Y.; et al. The Megamaser Cosmology Project. XIII. Combined Hubble Constant Constraints. *ApJ* **2020**, *891*, L1, [arXiv:astro-ph.CO/2001.09213]. <https://doi.org/10.3847/2041-8213/ab75f0>.
- Schombert, J.; McGaugh, S.; Lelli, F. Using the Baryonic Tully-Fisher Relation to Measure H_0 . *AJ* **2020**, *160*, 71, [arXiv:astro-ph.CO/2006.08615]. <https://doi.org/10.3847/1538-3881/ab9d88>.
- Blakeslee, J.P.; Jensen, J.B.; Ma, C.P.; Milne, P.A.; Greene, J.E. The Hubble Constant from Infrared Surface Brightness Fluctuation Distances. *ApJ* **2021**, *911*, 65, [arXiv:astro-ph.CO/2101.02221]. <https://doi.org/10.3847/1538-4357/abe86a>.
- Riess, A.G.; Yuan, W.; Macri, L.M.; Scolnic, D.; Brout, D.; Casertano, S.; Jones, D.O.; Murakami, Y.; Anand, G.S.; Breuval, L.; et al. A Comprehensive Measurement of the Local Value of the Hubble Constant with 1 km s⁻¹ Mpc⁻¹ Uncertainty from the Hubble Space Telescope and the SHOES Team. *ApJ* **2022**, *934*, L7, [arXiv:astro-ph.CO/2112.04510]. <https://doi.org/10.3847/2041-8213/ac5c5b>.

20. Tully, R.B.; Kourkchi, E.; Courtois, H.M.; Anand, G.S.; Blakeslee, J.P.; Brout, D.; Jaeger, T.d.; Dupuy, A.; Guinet, D.; Howlett, C.; et al. Cosmicflows-4. *ApJ* **2023**, *944*, 94, [arXiv:astro-ph.CO/2209.11238]. <https://doi.org/10.3847/1538-4357/ac94d8>.
21. Planck Collaboration.; Aghanim, N.; Akrami, Y.; Ashdown, M.; Aumont, J.; Baccigalupi, C.; Ballardini, M.; Banday, A.J.; Barreiro, R.B.; Bartolo, N.; et al. Planck 2018 results. VI. Cosmological parameters. *A&A* **2020**, *641*, A6, [arXiv:astro-ph.CO/1807.06209]. <https://doi.org/10.1051/0004-6361/201833910>.
22. Spergel, D.N.; Bean, R.; Doré, O.; Nolta, M.R.; Bennett, C.L.; Dunkley, J.; Hinshaw, G.; Jarosik, N.; Komatsu, E.; Page, L.; et al. Three-Year Wilkinson Microwave Anisotropy Probe (WMAP) Observations: Implications for Cosmology. *ApJS* **2007**, *170*, 377–408, [arXiv:astro-ph/astro-ph/0603449]. <https://doi.org/10.1086/513700>.
23. Cole, S.; Percival, W.J.; Peacock, J.A.; Norberg, P.; Baugh, C.M.; Frenk, C.S.; Baldry, I.; Bland-Hawthorn, J.; Bridges, T.; Cannon, R.; et al. The 2dF Galaxy Redshift Survey: power-spectrum analysis of the final data set and cosmological implications. *MNRAS* **2005**, *362*, 505–534, [arXiv:astro-ph/astro-ph/0501174]. <https://doi.org/10.1111/j.1365-2966.2005.09318.x>.
24. Mantz, A.B.; Morris, R.G.; Allen, S.W.; Canning, R.E.A.; Baumont, L.; Benson, B.; Bleem, L.E.; Ehlert, S.R.; Floyd, B.; Herbonnet, R.; et al. Cosmological constraints from gas mass fractions of massive, relaxed galaxy clusters. *MNRAS* **2022**, *510*, 131–145, [arXiv:astro-ph.CO/2111.09343]. <https://doi.org/10.1093/mnras/stab3390>.
25. Ying, J.M.; Chaboyer, B.; Boudreaux, E.M.; Slaughter, C.; Boylan-Kolchin, M.; Weisz, D. The Absolute Age of M92. *AJ* **2023**, *166*, 18, [arXiv:astro-ph.SR/2306.02180]. <https://doi.org/10.3847/1538-3881/acd9b1>.
26. Mohayaee, R.; Tully, R.B. The Cosmological Mean Density and Its Local Variations Probed by Peculiar Velocities. *ApJ* **2005**, *635*, L113–L116, [arXiv:astro-ph/astro-ph/0509313]. <https://doi.org/10.1086/499774>.
27. Shaya, E.J.; Tully, R.B.; Hoffman, Y.; Pomarède, D. Action Dynamics of the Local Supercluster. *ApJ* **2017**, *850*, 207, [arXiv:astro-ph.CO/1710.08935]. <https://doi.org/10.3847/1538-4357/aa9525>.
28. Battye, R.A.; Charnock, T.; Moss, A. Tension between the power spectrum of density perturbations measured on large and small scales. *Phys. Rev. D* **2015**, *91*, 103508, [arXiv:astro-ph.CO/1409.2769]. <https://doi.org/10.1103/PhysRevD.91.103508>.
29. Abbott, T.M.C.; Aguena, M.; Alarcon, A.; Allam, S.; Alves, O.; Amon, A.; Andrade-Oliveira, F.; Annis, J.; Avila, S.; Bacon, D.; et al. Dark Energy Survey Year 3 results: Cosmological constraints from galaxy clustering and weak lensing. *Phys. Rev. D* **2022**, *105*, 023520, [arXiv:astro-ph.CO/2105.13549]. <https://doi.org/10.1103/PhysRevD.105.023520>.
30. Lange, J.U.; Hearin, A.P.; Leauthaud, A.; van den Bosch, F.C.; Xhakaj, E.; Guo, H.; Wechsler, R.H.; DeRose, J. Constraints on S_8 from a full-scale and full-shape analysis of redshift-space clustering and galaxy-galaxy lensing in BOSS. *MNRAS* **2023**, *520*, 5373–5393, [arXiv:astro-ph.CO/2301.08692]. <https://doi.org/10.1093/mnras/stad473>.
31. McGaugh, S.S. Confrontation of Modified Newtonian Dynamics Predictions with Wilkinson Microwave Anisotropy Probe First Year Data. *ApJ* **2004**, *611*, 26–39, [arXiv:astro-ph/astro-ph/0312570]. <https://doi.org/10.1086/421895>.
32. Cyburt, R.H.; Fields, B.D.; Olive, K.A. An update on the big bang nucleosynthesis prediction for ${}^7\text{Li}$: the problem worsens. *JCAP* **2008**, *2008*, 012, [arXiv:astro-ph/0808.2818]. <https://doi.org/10.1088/1475-7516/2008/11/012>.
33. Freedman, W.L. Measurements of the Hubble Constant: Tensions in Perspective. *ApJ* **2021**, *919*, 16, [arXiv:astro-ph.CO/2106.15656]. <https://doi.org/10.3847/1538-4357/ac0e95>.
34. Uddin, S.A.; Burns, C.R.; Phillips, M.M.; Suntzeff, N.B.; Freedman, W.L.; Brown, P.J.; Morrell, N.; Hamuy, M.; Krisciunas, K.; Wang, L.; et al. Carnegie Supernova Project-I and -II: Measurements of H_0 using Cepheid, TRGB, and SBF Distance Calibration to Type Ia Supernovae. *arXiv e-prints* **2023**, p. arXiv:2308.01875, [arXiv:astro-ph.CO/2308.01875]. <https://doi.org/10.48550/arXiv.2308.01875>.
35. Komatsu, E.; Dunkley, J.; Nolta, M.R.; Bennett, C.L.; Gold, B.; Hinshaw, G.; Jarosik, N.; Larson, D.; Limon, M.; Page, L.; et al. Five-Year Wilkinson Microwave Anisotropy Probe Observations: Cosmological Interpretation. *ApJ Suppl. Ser.* **2009**, *180*, 330–376. <https://doi.org/10.1088/0067-0049/180/2/330>.
36. Komatsu, E.; Smith, K.M.; Dunkley, J.; Bennett, C.L.; Gold, B.; Hinshaw, G.; Jarosik, N.; Larson, D.; Nolta, M.R.; Page, L.; et al. Seven-year Wilkinson Microwave Anisotropy Probe (WMAP) Observations: Cosmological Interpretation. *ApJS* **2011**, *192*, 18, [arXiv:astro-ph.CO/1001.4538]. <https://doi.org/10.1088/0067-0049/192/2/18>.
37. Hinshaw, G.; Larson, D.; Komatsu, E.; Spergel, D.N.; Bennett, C.L.; Dunkley, J.; Nolta, M.R.; Halpern, M.; Hill, R.S.; Odegard, N.; et al. Nine-year Wilkinson Microwave Anisotropy Probe (WMAP) Observations: Cosmological Parameter Results. *ApJS* **2013**, *208*, 19, [arXiv:astro-ph.CO/1212.5226]. <https://doi.org/10.1088/0067-0049/208/2/19>.
38. Planck Collaboration.; Ade, P.A.R.; Aghanim, N.; Armitage-Caplan, C.; Arnaud, M.; Ashdown, M.; Atrio-Barandela, F.; Aumont, J.; Baccigalupi, C.; Banday, A.J.; et al. Planck 2013 results. XVI. Cosmological parameters. *A&A* **2014**, *571*, A16, [arXiv:astro-ph.CO/1303.5076]. <https://doi.org/10.1051/0004-6361/201321591>.
39. Yung, L.Y.A.; Somerville, R.S.; Popping, G.; Finkelstein, S.L.; Ferguson, H.C.; Davé, R. Semi-analytic forecasts for JWST - II. Physical properties and scaling relations for galaxies at $z = 4-10$. *MNRAS* **2019**, *490*, 2855–2879, [arXiv:astro-ph.GA/1901.05964]. <https://doi.org/10.1093/mnras/stz2755>.
40. Stefanon, M.; Bouwens, R.J.; Labbé, I.; Illingworth, G.D.; Gonzalez, V.; Oesch, P.A. Galaxy Stellar Mass Functions from $z = 10$ to $z = 6$ using the Deepest Spitzer/Infrared Array Camera Data: No Significant Evolution in the Stellar-to-halo Mass Ratio of Galaxies in the First Gigayear of Cosmic Time. *ApJ* **2021**, *922*, 29, [arXiv:astro-ph.GA/2103.16571]. <https://doi.org/10.3847/1538-4357/ac1bb6>.

41. Vogelsberger, M.; Genel, S.; Springel, V.; Torrey, P.; Sijacki, D.; Xu, D.; Snyder, G.; Bird, S.; Nelson, D.; Hernquist, L. Properties of galaxies reproduced by a hydrodynamic simulation. *Nature* **2014**, *509*, 177–182, [arXiv:astro-ph.CO/1405.1418]. <https://doi.org/10.1038/nature13316>.
42. Henriques, B.M.B.; White, S.D.M.; Thomas, P.A.; Angulo, R.; Guo, Q.; Lemson, G.; Springel, V.; Overzier, R. Galaxy formation in the Planck cosmology - I. Matching the observed evolution of star formation rates, colours and stellar masses. *MNRAS* **2015**, *451*, 2663–2680, [arXiv:astro-ph.GA/1410.0365]. <https://doi.org/10.1093/mnras/stv705>.
43. Steinhardt, C.L.; Capak, P.; Masters, D.; Speagle, J.S. The Impossibly Early Galaxy Problem. *ApJ* **2016**, *824*, 21, [arXiv:astro-ph.GA/1506.01377]. <https://doi.org/10.3847/0004-637X/824/1/21>.
44. Franck, J.R.; McGaugh, S.S. Spitzer’s View of the Candidate Cluster and Protocluster Catalog (CCPC). *ApJ* **2017**, *836*, 136, [arXiv:astro-ph.GA/1701.05560]. <https://doi.org/10.3847/1538-4357/836/1/136>.
45. Nanayakkara, T.; Glazebrook, K.; Jacobs, C.; Schreiber, C.; Brammer, G.; Esdaile, J.; Kacprzak, G.G.; Labbe, I.; Lagos, C.; Marchesini, D.; et al. A population of faint, old, and massive quiescent galaxies at $3 < z < 4$ revealed by JWST NIRSpec Spectroscopy. *arXiv e-prints* **2022**, p. arXiv:2212.11638, [arXiv:astro-ph.GA/2212.11638]. <https://doi.org/10.48550/arXiv.2212.11638>.
46. Glazebrook, K.; Nanayakkara, T.; Schreiber, C.; Lagos, C.; Kawinwanichakij, L.; Jacobs, C.; Chittenden, H.; Brammer, G.; Kacprzak, G.G.; Labbe, I.; et al. An extraordinarily massive galaxy that formed its stars at *z*sim11. *arXiv e-prints* **2023**, p. arXiv:2308.05606, [arXiv:astro-ph.GA/2308.05606]. <https://doi.org/10.48550/arXiv.2308.05606>.
47. Sanders, R.H. Cosmology with modified Newtonian dynamics (MOND). *MNRAS* **1998**, *296*, 1009–1018, [arXiv:astro-ph/astro-ph/9710335]. <https://doi.org/10.1046/j.1365-8711.1998.01459.x>.
48. Boylan-Kolchin, M. Stress testing Λ CDM with high-redshift galaxy candidates. *Nature Astronomy* **2023**, *7*, 731–735, [arXiv:astro-ph.CO/2208.01611]. <https://doi.org/10.1038/s41550-023-01937-7>.
49. Haslbauer, M.; Kroupa, P.; Zonoozi, A.H.; Hagi, H. Has JWST Already Falsified Dark-matter-driven Galaxy Formation? *ApJ* **2022**, *939*, L31, [arXiv:astro-ph.GA/2210.14915]. <https://doi.org/10.3847/2041-8213/ac9a50>.
50. Labbé, I.; van Dokkum, P.; Nelson, E.; Bezanson, R.; Suess, K.A.; Leja, J.; Brammer, G.; Whitaker, K.; Mathews, E.; Stefanon, M.; et al. A population of red candidate massive galaxies 600 Myr after the Big Bang. *Nature* **2023**, *616*, 266–269, [arXiv:astro-ph.GA/2207.12446]. <https://doi.org/10.1038/s41586-023-05786-2>.
51. Naidu, R.P.; Oesch, P.A.; van Dokkum, P.; Nelson, E.J.; Suess, K.A.; Brammer, G.; Whitaker, K.E.; Illingworth, G.; Bouwens, R.; Tacchella, S.; et al. Two Remarkably Luminous Galaxy Candidates at $z \approx 10$ –12 Revealed by JWST. *ApJ* **2022**, *940*, L14, [arXiv:astro-ph.GA/2207.09434]. <https://doi.org/10.3847/2041-8213/ac9b22>.
52. Finkelstein, S.L.; Bagley, M.B.; Haro, P.A.; Dickinson, M.; Ferguson, H.C.; Kartaltepe, J.S.; Papovich, C.; Burgarella, D.; Kocevski, D.D.; Huertas-Company, M.; et al. A Long Time Ago in a Galaxy Far, Far Away: A Candidate $z \approx 12$ Galaxy in Early JWST CEERS Imaging. *ApJ* **2022**, *940*, L55, [arXiv:astro-ph.GA/2207.12474]. <https://doi.org/10.3847/2041-8213/ac966e>.
53. Atek, H.; Shuntov, M.; Furtak, L.J.; Richard, J.; Kneib, J.P.; Mahler, G.; Zitrin, A.; McCracken, H.J.; Charlot, S.; Chevillard, J.; et al. Revealing galaxy candidates out to $z = 16$ with JWST observations of the lensing cluster SMACS0723. *MNRAS* **2023**, *519*, 1201–1220, [arXiv:astro-ph.GA/2207.12338]. <https://doi.org/10.1093/mnras/stac3144>.
54. Adams, N.J.; Conselice, C.J.; Ferreira, L.; Austin, D.; Trussler, J.A.A.; Juodžbalis, I.; Wilkins, S.M.; Caruana, J.; Dayal, P.; Verma, A.; et al. Discovery and properties of ultra-high redshift galaxies ($9 < z < 12$) in the JWST ERO SMACS 0723 Field. *MNRAS* **2023**, *518*, 4755–4766, [arXiv:astro-ph.GA/2207.11217]. <https://doi.org/10.1093/mnras/stac3347>.
55. Casey, C.M.; Akins, H.B.; Shuntov, M.; Ilbert, O.; Paquereau, L.; Franco, M.; Hayward, C.C.; Finkelstein, S.L.; Boylan-Kolchin, M.; Robertson, B.E.; et al. COSMOS-Web: Intrinsically Luminous *z*sim10 Galaxy Candidates Test Early Stellar Mass Assembly. *arXiv e-prints* **2023**, p. arXiv:2308.10932, [arXiv:astro-ph.GA/2308.10932]. <https://doi.org/10.48550/arXiv.2308.10932>.
56. Yung, L.Y.A.; Somerville, R.S.; Finkelstein, S.L.; Wilkins, S.M.; Gardner, J.P. Are the ultra-high-redshift galaxies at $z > 10$ surprising in the context of standard galaxy formation models? *MNRAS* **2023**, [arXiv:astro-ph.GA/2304.04348]. <https://doi.org/10.1093/mnras/stad3484>.
57. Harikane, Y.; Ouchi, M.; Oguri, M.; Ono, Y.; Nakajima, K.; Isobe, Y.; Umeda, H.; Mawatari, K.; Zhang, Y. A Comprehensive Study of Galaxies at $z \approx 9$ –16 Found in the Early JWST Data: Ultraviolet Luminosity Functions and Cosmic Star Formation History at the Pre-reionization Epoch. *ApJS* **2023**, *265*, 5, [arXiv:astro-ph.GA/2208.01612]. <https://doi.org/10.3847/1538-4365/acaaa9>.
58. Finkelstein, S.L.; Leung, G.C.K.; Bagley, M.B.; Dickinson, M.; Ferguson, H.C.; Papovich, C.; Akins, H.B.; Arrabal Haro, P.; Dave, R.; Dekel, A.; et al. The Complete CEERS Early Universe Galaxy Sample: A Surprisingly Slow Evolution of the Space Density of Bright Galaxies at $z \approx 8.5$ –14.5. *arXiv e-prints* **2023**, p. arXiv:2311.04279, [arXiv:astro-ph.GA/2311.04279]. <https://doi.org/10.48550/arXiv.2311.04279>.
59. McGaugh, S.S. Early Galaxy Formation and the Hubble Constant Tension. *Research Notes of the American Astronomical Society* **2023**, *7*, 20. <https://doi.org/10.3847/2515-5172/acba9a>.
60. Planck Collaboration.; Aghanim, N.; Akrami, Y.; Ashdown, M.; Aumont, J.; Baccigalupi, C.; Ballardini, M.; Banday, A.J.; Barreiro, R.B.; Bartolo, N.; et al. Planck 2018 results. V. CMB power spectra and likelihoods. *A&A* **2020**, *641*, A5, [arXiv:astro-ph.CO/1907.12875]. <https://doi.org/10.1051/0004-6361/201936386>.
61. Lewis, A.; Challinor, A. CAMB: Code for Anisotropies in the Microwave Background. Astrophysics Source Code Library, record ascl:1102.026, 2011, [1102.026].
62. McGaugh, S.S. A tale of two paradigms: the mutual incommensurability of Λ CDM and MOND. *Canadian Journal of Physics* **2015**, *93*, 250–259, [arXiv:astro-ph.CO/1404.7525]. <https://doi.org/10.1139/cjp-2014-0203>.